Dalton Transactions

PAPER

View Article Online
View Journal | View Issue

Cite this: *Dalton Trans.*, 2016, **45**, 15180

Peripheral halo-functionalization in [Cu(N^N)(P^P)]$^+$ emitters: influence on the performances of light-emitting electrochemical cells†

Fabian Brunner,[a] Laura Martínez-Sarti,[b] Sarah Keller,[a] Antonio Pertegás,[b] Alessandro Prescimone,[a] Edwin C. Constable,[a] Henk J. Bolink*[b,c] and Catherine E. Housecroft*[a]

A series of heteroleptic [Cu(N^N)(P^P)][PF_6] complexes is described in which P^P = bis(2-(diphenylphosphino)phenyl)ether (POP) or 4,5-bis(diphenylphosphino)-9,9-dimethylxanthene (xantphos) and N^N = 4,4′-diphenyl-6,6′-dimethyl-2,2′-bipyridine substituted in the 4-position of the phenyl groups with atom X (N^N = **1** has X = F, **2** has X = Cl, **3** has X = Br, **4** has X = I; the benchmark N^N ligand with X = H is **5**). These complexes have been characterized by multinuclear NMR spectroscopy, mass spectrometry, elemental analyses and cyclic voltammetry; representative single crystal structures are also reported. The solution absorption spectra are characterized by high energy bands (arising from ligand-centred transitions) which are red-shifted on going from X = H to X = I, and a broad metal-to-ligand charge transfer band with λ_{max} in the range 387–395 nm. The ten complexes are yellow emitters in solution and yellow or yellow-orange emitters in the solid-state. For a given N^N ligand, the solution photoluminescence (PL) spectra show no significant change on going from [Cu(N^N)(POP)]$^+$ to [Cu(N^N)(xantphos)]$^+$; introducing the iodo-functionality into the N^N domain leads to a red-shift in λ_{em}^{max} compared to the complexes with the benchmark N^N ligand **5**. In the solid state, [Cu(**1**)(POP)][PF_6] and [Cu(**1**)(xantphos)][PF_6] (fluoro-substituent) exhibit the highest PL quantum yields (74 and 25%, respectively) with values of $\tau_{1/2}$ = 11.1 and 5.8 μs, respectively. Light-emitting electrochemical cells (LECs) with [Cu(N^N)(P^P)][PF_6] complexes in the emissive layer have been tested. Using a block-wave pulsed current driving mode, the best performing device employed [Cu(**1**)(xantphos)]$^+$ and this showed a maximum luminance (Lum_{max}) of 129 cd m^{-2} and a device lifetime ($t_{1/2}$) of 54 h; however, the turn-on time (time to reach Lum_{max}) was 4.1 h. Trends in performance data reveal that the introduction of fluoro-groups is beneficial, but that the incorporation of heavier halo-substituents leads to poor devices, probably due to a detrimental effect on charge transport; LECs with the iodo-functionalized N^N ligand **4** failed to show any electroluminescence after 50 h.

Received 5th July 2016,
Accepted 16th August 2016

DOI: 10.1039/c6dt02665f

www.rsc.org/dalton

Introduction

Light-emitting electrochemical cells (LECs)[1–4] based on polymers,[5,6] small molecules[7–11] and ionic transition-metal complexes (iTMCs)[1,12–14] are an emerging technology[15] with potential for cheap and robust device fabrication methods including the printing of flexible LECs.[16] Although Ir-iTMCs (and to a lesser extent Ru-iTMCs[17–20]) are the light-emitting components of many LECs, Cu-iTMCs are of growing importance. Copper has emerged as a promising alternative to less Earth abundant metals both in LECs and for solar energy conversion.[21] Among the copper(I) complexes investigated in LECs, the most ubiquitous are those of type [Cu(N^N)(P^P)]$^+$ (P^P and N^N = chelating bis(phosphine) and diimine ligands, respectively).[22–36] The synthesis of heteroleptic [Cu(N^N)(P^P)]$^+$ complexes is straightforward, allowing rapid screening of compound families for promising photoluminescence (PL) properties prior to testing in the LEC configuration. It has also been reported that some Cu-iTMCs exhibit thermally activated delayed fluorescence (TADF) giving

[a]*Department of Chemistry, University of Basel, Spitalstrasse 51, CH-4056 Basel, Switzerland. E-mail: catherine.housecroft@unibas.ch*
[b]*Instituto de Ciencia Molecular, Universidad de Valencia, Catedrático José Beltrán 2, Paterna, E-46980, Spain. E-mail: henk.bolink@uv.es*
[c]*Fundació General de la Universitat de Valencia (FGUV), PO Box 22085, Valencia, Spain*

†Electronic supplementary information (ESI) available: Fig. S1–S3: additional structural data; Fig. S4: absorption spectra of [Cu(N^N)(POP)][PF_6]; Fig. S5–S8: solid-state and thin film emission spectra; Fig. S9: EL spectra for LECs; Fig. S10–14: device performances; Table S1: photoluminescence lifetimes. CCDC 1486906–1486911. For ESI and crystallographic data in CIF or other electronic format see DOI: 10.1039/c6dt02665f

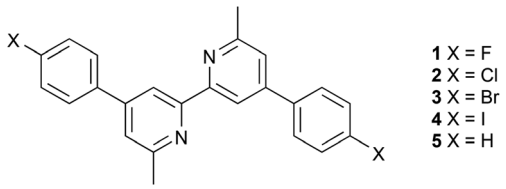

Scheme 1 Structures of the N^N ligands **1–5**.

access to a singlet-harvesting effect which could increase the overall device performance.[37–42]

A major design challenge for Cu-iTMCs is the combination of high efficiency and long device lifetimes with long-term device stability. For $[Cu(N^N)(P^P)]^+$ complexes in which P^P is bis(2-(diphenylphosphino)phenyl)ether (POP) or 4,5-bis(diphenylphosphino)-9,9-dimethylxanthene (xantphos) and N^N is 2,2′-bipyridine (bpy) a 6- or 6,6′-substituted bpy, we have demonstrated that the LEC efficacy and device lifetime can be tuned by simple variations of the 6- or 6,6′-substituents, whilst maintaining acceptable turn-on times.[22,24] Emission properties improve on going from $[Cu(bpy)(POP)]^+$, to $[Cu(Mebpy)(POP)]^+$ (Mebpy = 6-methyl-2,2′-bipyridine) to $[Cu(Me_2bpy)(POP)]^+$ (Me_2bpy = 6,6′-dimethyl-2,2′-bipyridine), in line with the observation of McMillin and coworkers of enhanced PL on increasing the number of 2,9-substituents in the phen (phen = 1,10-phenanthroline) domain in $[Cu(phen)(POP)]^+$.[43] Changing from POP to xantphos while maintaining N^N = Me_2bpy leads to a LEC with a maximum efficacy of 3.0 cd A^{-1} (luminance = 145 cd m^{-2}) and a device lifetime (the time to reach one-half of the maximum luminance) of 1 h. On going from $[Cu(Me_2bpy)(xantphos)]^+$ to $[Cu(Mebpy)(xantphos)]^+$, the device lifetime increases to >15 h but the efficacy drops to 1.9 cd A^{-1}.[22] The photoluminescence of copper(I) complexes is strongly influenced by the surrounding environment,[44] and the presence of xantphos in place of POP leads to copper(I) complexes having a higher degree of rigidity which should lead to a stronger photoluminescence. In the present investigation, we retain the optimized 6,6′-dimethyl substitution pattern in the N^N domain of the Cu-iTMC and investigate the introduction of additional functionality at the 4- and 4′-positions of the bpy. We have investigated the N^N ligands **1–4** shown in Scheme 1 with peripheral halogroups; **5** was included as a benchmark. We recently demonstrated that, contrary to rational dye-design strategies, the incorporation of ligand **4** in copper-based dye-sensitized solar cells lead to remarkably high photoconversion efficiencies.[45] In view of these unexpected effects which are not readily explained in terms of electronic influences, we were prompted to investigate the halo-functionalized N^N ligands **1–4** in $[Cu(N^N)(P^P)]^+$ complexes in LECs in a systematic manner.

Experimental

General

^1H, ^{13}C and ^{31}P NMR spectra were recorded using a Bruker Avance III-500 NMR spectrometer. ^1H and ^{13}C NMR chemical shifts were referenced to the residual solvent peaks with respect to δ(TMS) = 0 ppm and ^{31}P NMR chemical shifts with respect to δ(85% aqueous H_3PO_4) = 0 ppm. Solution absorption and emission spectra were measured using an Agilent 8453 spectrophotometer and a Shimadzu RF-5301PC spectrofluorometer, respectively; a Bruker esquire 3000plus instrument was used to record electrospray ionization (ESI) mass spectra. Quantum yields (CH_2Cl_2 solution and powder) were measured using a Hamamatsu absolute photoluminescence (PL) quantum yield spectrometer C11347 Quantaurus-QY. Emission lifetimes and powder emission spectra were measured with a Hamamatsu Compact Fluorescence lifetime Spectrometer C11367 Quantaurus-Tau, using an LED light source with λ_{exc} = 365 nm. Quantum yields and PL emission spectra in thin films were recorded using a Hamamatsu absolute quantum yield C9920. The preparation of the thin film samples consisted of deposition on a quartz plate (1 cm^2) of the complex with addition of the ionic liquid 1-ethyl-3-methylimidazolium hexafluoridophosphate [Emim][PF_6].

Compounds **1–5** were prepared using reported methods[45–47] and the NMR spectroscopic data matched with those reported. POP was purchased from Acros and xantphos from Fluorochem. $[Cu(MeCN)_4][PF_6]$ was prepared by the published method.[48]

[Cu(1)(POP)][PF_6]. $[Cu(MeCN)_4][PF_6]$ (261 mg, 0.70 mmol) and POP (415 mg, 0.70 mmol) were dissolved in CH_2Cl_2 (80 ml) and stirred for 2 h at room temperature. Compound **1** (261 mg, 0.70 mmol) was added and the mixture was stirred for 2 h at room temperature during which it turned yellow. The reaction mixture was filtered, the solvent was removed from the filtrate, and the crude material was washed with hexane (2 × 50 ml). It was redissolved in a small amount of acetone before being layered with Et_2O. After 2 days, yellow crystals had formed. They were collected, ground to a powder and dried under vacuum to give yellow [Cu(**1**)(POP)][PF_6] (522 mg, 0.47 mmol, 66%). ^1H NMR (500 MHz, acetone-d_6) δ/ppm: 8.70 (d, J = 1.7 Hz, 2H, H^{A3}), 8.02 (m, 4H, H^{B2}), 7.76 (d, J = 1.6 Hz, 2H, H^{A5}), 7.45 (m, 2H, H^{C5}), 7.38–7.33 (overlapping m, 8H, H^{B3+D4}), 7.32–7.27 (overlapping m, 4H, H^{C3+C4}), 7.22 (t, J = 7.7 Hz, 8H, H^{D3}), 7.17 (m, 8H, H^{D2}), 7.08 (m, 2H, H^{C6}), 2.41 (s, 6H, H^a). ^{13}C NMR (126 MHz, acetone-d_6) δ/ppm: 164.8 (d, J_{FC} = 249 Hz, C^{B4}), 160.0 (C^{A6}), 159.1 (t, J_{PC} = 6.0 Hz, C^{C1}), 154.1 (C^{A2}), 150.6 (C^{A4}), 134.6 (C^{C3}), 134.1 (C^{B1}), 134.0 (t, J_{PC} = 7.8 Hz, C^{D2}), 133.3 (C^{C5}), 132.9 (t, J_{PC} = 16.2 Hz, C^{D1}), 130.8 (C^{D4}), 130.7 (d, J_{FC} = 8.6 Hz, C^{B2}), 129.6 (t, J_{PC} = 4.9 Hz, C^{D3}), 126.2 (t, J_{PC} = 2.4 Hz, C^{C4}), 126.2 (t, J_{PC} = 13.7 Hz, C^{C2}), 124.7 (C^{A5}), 121.1 (C^{C6}), 119.0 (C^{A3}), 117.0 (d, J_{FC} = 21.9 Hz, C^{B3}), 26.9 (C^a). ^{31}P NMR (202 MHz, acetone-d_6) δ/ppm −13.6 (broad, FWHM = 180 Hz), −144.5 (septet, J_{PF} = 710 Hz, $[PF_6]^-$). ESI MS: m/z 973.3 $[M - PF_6]^+$ (base peak, calc. 973.2). UV-vis (CH_2Cl_2, 2.5 × 10^{-5} mol dm^{-3}): λ/nm (ε/dm^3 mol^{-1} cm^{-1}) 228 (52 000), 263 (53 700), 309sh (24 000), 388 (4600). Found: C 64.14, H 4.67, N 2.74; $C_{60}H_{46}CuF_8N_2OP_3$ requires C 64.37, H 4.14, N 2.50%.

[Cu(1)(xantphos)][PF_6]. $[Cu(MeCN)_4][PF_6]$ (37.3 mg, 0.10 mmol) was dissolved in CH_2Cl_2 (5 ml). A suspension of xantphos (59 mg, 0.1 mmol) and **1** (37.2 mg, 0.10 mmol) in

CH_2Cl_2 (5 ml) was added and the mixture turned red and then orange while it was stirred for 2 h at RT. The solution was filtered, the solvent was removed and the crude material was ground to a powder, washed with hexane (2 × 15 ml) and dried under vacuum to give [Cu(**1**)(xantphos)][PF_6] (176 mg, 0.15 mmol, 76%) as a yellow solid. ^{1}H NMR (500 MHz, acetone-d_6) δ/ppm: 8.61 (d, J = 1.7 Hz, 2H, H^{A3}), 7.98 (m, 4H, H^{B2}), 7.85 (dd, J = 7.8 Hz, J = 1.4 Hz, 2H, H^{C5}), 7.71 (d, J = 1.6 Hz, 2H, H^{A5}), 7.41 (m, 4H, H^{D4}), 7.38–7.31 (overlapping m, 6H, H^{B3+C4}), 7.27–7.21 (overlapping m, 16H, H^{D2+D3}), 7.01 (m, 2H, H^{C3}), 2.23 (s, 6H, H^a), 1.77 (s, 6H, H^b). ^{13}C NMR (126 MHz, acetone-d_6) δ/ppm: 164.8 (d, J_{FC} = 249 Hz, C^{B4}), 159.5 (C^{A6}), 155.9 (t, J_{PC} = 6.6 Hz, C^{C1}), 153.9 (C^{A2}), 150.6 (C^{A4}), 134.8 (C^{C6}), 134.1 (t, J_{PC} = 7.7 Hz, C^{D2}), 134.0 (d, J_{FC} = 3.2 Hz, C^{B1}), 132.5 (t, J_{PC} = 16.1 Hz, C^{D1}), 131.2 (C^{C3}), 130.6 (d, J_{FC} = 8.7 Hz, C^{B2}), 131.0 (C^{D4}), 129.8 (t, J_{PC} = 4.5 Hz, C^{D3}), 128.1 (C^{C5}), 126.4 (C^{C4}), 124.2 (C^{A5}), 122.7 (t, J_{PC} = 13.0 Hz, C^{C2}), 119.0 (C^{A3}), 117.0 (d, J_{PC} = 21.9 Hz, C^{B3}), 36.9 (C^{Cq}), 28.7 (C^b), 27.1 (C^a). ^{31}P NMR (202 MHz, acetone-d_6) δ/ppm −13.6 (broad, FWHM = 170 Hz), −144.5 (septet, J_{PF} = 710 Hz, $[PF_6]^-$). ESI MS: m/z 1013.3 $[M - PF_6]^+$ (base peak, calc. 1013.3). UV-vis (CH_2Cl_2, 2.5 × 10^{-5} mol dm^{-3}): λ/nm (ε/dm^3 mol^{-1} cm^{-1}) 229 (58 000), 266 (63 000), 312sh (24 000), 391 (4700). Found: C 65.45, H 4.71, N 2.67; $C_{63}H_{50}CuF_8N_2OP_3$ requires C 65.26, H 4.35, N 2.42%.

[Cu(2)(POP)][PF_6]. [Cu(MeCN)$_4$][PF_6] (93.2 mg, 0.25 mmol) and POP (135 mg, 0.25 mmol) were dissolved in CH_2Cl_2 (30 ml) and the mixture was stirred for 1.5 h at room temperature. Compound **2** (101 mg, 0.25 mmol) was added and stirring was continued for 1.5 h. The yellow solution was filtered and the solvent was removed from the filtrate. The solid material was washed with hexane (2 × 30 ml) and dried under vacuum to give [Cu(**2**)(POP)][PF_6] (277 mg, 0.24 mmol, 96%) as a yellow solid. ^{1}H NMR (500 MHz, acetone-d_6) δ/ppm: 8.71 (d, J = 1.7 Hz, 2H, H^{A3}), 7.97 (m, 4H, H^{B2}), 7.78 (d, J = 1.6 Hz, 2H, H^{A5}), 7.62 (m, 4H, H^{B3}), 7.50 (m, 2H, H^{C5}), 7.35 (t, J = 7.3 Hz, 4H, H^{D4}), 7.32–7.28 (overlapping m, 4H, H^{C3+C4}), 7.22 (t, J = 7.8 Hz, 8H, H^{D3}), 7.17 (m, 8H, H^{D2}), 7.06 (m, 2H, H^{C6}), 2.41 (s, 6H, H^a). ^{13}C NMR (126 MHz, acetone-d_6) δ/ppm: 160.2 (C^{A6}), 159.3 (t, J_{PC} = 5.9 Hz, C^{C1}), 154.3 (C^{A2}), 150.5 (C^{A4}), 136.7 (C^{B4}), 136.6 (C^{B1}) 134.7 (C^{C3}), 134.2 (t, J_{PC} = 7.8 Hz, C^{D2}), 133.5 (C^{C5}), 133.0 (t, J_{PC} = 16.2 Hz, C^{D1}), 131.0 (C^{D4}), 130.4 (C^{B3}), 130.2 (C^{B2}), 129.8 (t, J_{PC} = 4.6 Hz, C^{D3}), 126.4 (overlapping m, C^{C2+C4}), 124.8 (C^{A5}), 121.2 (C^{C6}), 119.3 (C^{A3}), 27.1 (C^a). ^{31}P NMR (202 MHz, acetone-d_6) δ/ppm −13.3 (broad, FWHM = 116 Hz), −144.5 (septet, J_{PF} = 710 Hz, $[PF_6]^-$). ESI MS: m/z 1007.2 $[M - PF_6]^+$ (base peak, calc. 1007.2). UV-vis (CH_2Cl_2, 2.5 × 10^{-5} mol dm^{-3}): λ/nm (ε/dm^3 mol^{-1} cm^{-1}) 228 (58 000), 269 (62 000), 312sh (28 000), 395 (5500). Found: C 62.33, H 4.38, N 2.66; $C_{60}H_{46}Cl_2CuF_6N_2OP_3$ requires C 62.54, H 4.02, N 2.43%.

[Cu(2)(xantphos)][PF_6]. [Cu(MeCN)$_4$][PF_6] (93.2 mg, 0.25 mmol) was dissolved in CH_2Cl_2 (15 ml). A suspension of xantphos (148 mg, 0.25 mmol) and **2** (101 mg, 0.25 mmol) in CH_2Cl_2 (25 ml) was added and the mixture turned red and then yellow while it was stirred for 1.5 h at room temperature. The solution was filtered, and the solvent was removed from the filtrate. The solid product was washed with hexane (2 × 30 ml) and dried under vacuum. [Cu(**2**)(xantphos)][PF_6] was isolated as a yellow solid (294 mg, 0.25 mmol, 98%). ^{1}H NMR (500 MHz, acetone-d_6) δ/ppm: 8.62 (d, J = 1.8 Hz, 2H, H^{A3}), 7.94 (m, 4H, H^{B2}), 7.85 (dd, J = 7.9 Hz, J = 1.4 Hz, 2H, H^{C5}), 7.74 (d, J = 1.6 Hz, 2H, H^{A5}), 7.60 (m, 4H, H^{B3}), 7.42 (m, 4H, H^{D4}), 7.33 (t, J = 7.7 Hz, 2H, H^{C4}), 7.27–7.20 (overlapping m, 16H, H^{D2+D3}), 7.01 (m, 2H, H^{C3}), 2.23 (s, 6H, H^a), 1.77 (s, 6H, H^b). ^{13}C NMR (126 MHz, acetone-d_6) δ/ppm: 159.8 (C^{A6}), 156.0 (t, J_{PC} = 6.5 Hz, C^{C1}), 154.0 (C^{A2}), 150.5 (C^{A4}), 136.7 (C^{B4}), 136.5 (C^{B1}), 135.0 (t, J_{PC} = 1.8 Hz, C^{C6}), 134.3 (t, J_{PC} = 7.7 Hz, C^{D2}), 132.7 (t, J_{PC} = 16.3 Hz, C^{D1}), 131.3 (C^{C3}), 131.2 (C^{D4}), 130.4 (C^{B3}), 130.2 (C^{B2}), 129.9 (t, J_{PC} = 4.5 Hz, C^{D3}), 128.9 (C^{C5}), 126.5 (C^{C4}), 124.4 (C^{A5}), 122.8 (t, J_{PC} = 12.7 Hz, C^{C2}), 119.2 (C^{A3}), 37.0 (C^{Cq}), 28.9 (C^b), 27.2 (C^a). ^{31}P NMR (202 MHz, acetone-d_6) δ/ppm −13.5 (broad, FWHM = 133 Hz), −144.5 (septet, J_{PF} = 710 Hz, $[PF_6]^-$). ESI MS: m/z 1047.2 $[M - PF_6]^+$ (base peak, calc. 1047.2). UV-vis (CH_2Cl_2, 2.5 × 10^{-5} mol dm^{-3}): λ/nm (ε/dm^3 mol^{-1} cm^{-1}) 227 (57 000), 271 (64 000), 315sh (24 000), 395 (5000). Found: C 63.49, H 4.59, N 2.64; $C_{63}H_{50}Cl_2CuF_6N_2OP_3$ requires C 63.46, H 4.23, N 2.35%.

[Cu(3)(POP)][PF_6]. [Cu(**3**)(POP)][PF_6] was prepared according to the procedure for [Cu(**2**)(POP)][PF_6] using [Cu(MeCN)$_4$][PF_6] (93 mg, 0.25 mmol), POP (135 mg, 0.25 mmol) and **3** (124 mg, 0.25 mmol). [Cu(**3**)(POP)][PF_6] was isolated as an orange solid (215 mg, 0.173 mmol, 69%). ^{1}H NMR (500 MHz, acetone-d_6) δ/ppm: 8.70 (d, J = 1.7 Hz, 2H, H^{A3}), 7.91 (m, 4H, H^{B3}), 7.78–7.75 (overlapping m, 6H, H^{A5+B2}), 7.45 (m, 2H, H^{C5}), 7.35 (t, J = 7.3 Hz, 4H, H^{D4}), 7.32–7.29 (overlapping m, 4H, H^{C3+C4}), 7.22 (t, J = 7.7 Hz, 8H, H^{D3}), 7.17 (m, 8H, H^{D2}), 7.07 (m, 2H, H^{C6}), 2.41 (s, 6H, H^a). ^{13}C NMR (126 MHz, acetone-d_6) δ/ppm: 160.3 (C^{A6}), 159.3 (t, J_{PC} = 6.0 Hz, C^{C1}), 154.3 (C^{A2}), 150.6 (C^{A4}), 137.0 (C^{B1}) 134.7 (C^{C3}), 134.2 (t, J_{PC} = 7.8 Hz, C^{D2}), 133.5 (C^{C5}), 133.0 (t, J_{PC} = 16.3 Hz, C^{D1}), 131.0 (C^{D4}), 130.4 (C^{B3}), 129.7 (t, J_{PC} = 4.6 Hz, C^{D3}), 126.3 (t, J_{PC} = 2.2 Hz, C^{C4}), 126.3 (t, J_{PC} = 14.0 Hz, C^{C2}) 125.0 (C^{B4}), 124.8 (C^{A5}), 121.2 (C^{C6}), 119.3 (C^{A3}), 27.1 (C^a). ^{31}P NMR (202 MHz, acetone-d_6) δ/ppm −13.6 (broad, FWHM = 136 Hz), −144.5 (septet, J_{PF} = 710 Hz, $[PF_6]^-$). ESI MS: m/z 1095.1 $[M - PF_6]^+$ (base peak, calc. 1095.1). UV-vis (CH_2Cl_2, 2.5 × 10^{-5} mol dm^{-3}): λ/nm (ε/dm^3 mol^{-1} cm^{-1}) 229 (54 000), 270 (57 900), 310sh (26 700), 393 (4900). Found: C 58.34, H 4.11, N 2.39; $C_{60}H_{46}Br_2CuF_6N_2OP_3$ requires C 58.06, H 3.74, N 2.23%.

[Cu(3)(xantphos)][PF_6]. [Cu(**3**)(xantphos)][PF_6] was prepared according to the procedure for [Cu(**2**)(xantphos)][PF_6] using [Cu(MeCN)$_4$][PF_6] (93 mg, 0.25 mmol), xantphos (148 mg, 0.25 mmol) and **3** (124 mg, 0.25 mmol). [Cu(**3**)(xantphos)][PF_6] (315 mg, 0.25 mmol, 98%) was isolated as an orange solid. ^{1}H NMR (500 MHz, acetone-d_6) δ/ppm: 8.61 (d, J = 1.7 Hz, 2H, H^{A3}), 7.88–7.84 (overlapping m, 6H, H^{B3+C5}), 7.75 (m, 4H, H^{B2}), 7.74 (d, J = 1.6 Hz, 2H, H^{A5}), 7.44–7.38 (m, 4H, H^{D4}), 7.33 (t, J = 7.7 Hz, 2H, H^{C4}), 7.26–7.20 (overlapping m, 16H, H^{D2+D3}), 7.00 (m, 2H, H^{C3}), 2.24 (s, 6H, H^a), 1.77 (s, 6H, H^b). ^{13}C NMR (126 MHz, acetone-d_6) δ/ppm: 159.8 (C^{A6}), 156.0 (t, J_{PC} = 6.5 Hz, C^{C1}), 154.0 (C^{A2}), 150.6 (C^{A4}), 136.9 (C^{B1}), 135.0 (C^{C6}), 134.3 (t, J_{PC} = 7.7 Hz, C^{D2}), 133.4 (C^{B2}), 132.6 (t, J_{PC} = 16.2 Hz, C^{D1}), 131.3 (C^{C3}), 131.2 (C^{D4}), 130.4 (C^{B3}), 129.9 (t, J_{PC} = 4.5 Hz,

C^{D3}), 128.9 (C^{C5}), 126.5 (C^{C4}), 125.1 (C^{B4}), 124.4 (C^{A5}), 122.8 (t, J_{PC} = 12.1 Hz, C^{C2}), 119.2 (C^{A3}), 37.1 (C^{Cq}), 28.9 (C^{b}), 27.2 (C^{a}). ^{31}P NMR (202 MHz, acetone-d_6) δ/ppm −13.5 (broad, FWHM = 138 Hz), −144.4 (septet, J_{PF} = 710 Hz, $[PF_6]^-$). ESI MS: m/z 1135.1 $[M - PF_6]^+$ (base peak, calc. 1135.1). UV-vis (CH_2Cl_2, 2.5 × 10^{-5} mol dm^{-3}): λ/nm (ε/dm^3 mol^{-1} cm^{-1}) 227 (54 000), 274 (63 000), 316sh (25 000), 395 (5400). Found: C 58.76, H 4.30, N 2.37; $C_{63}H_{50}Br_2CuF_6N_2OP_3$ requires C 59.05, H 3.93, N 2.19%.

[Cu(4)(POP)][PF$_6$]. [Cu(**4**)(POP)][PF_6] was prepared in an analogous manner to [Cu(**2**)(POP)][PF_6] starting with [Cu(MeCN)$_4$][PF_6] (93 mg, 0.25 mmol), POP (135 mg, 0.25 mmol) and **4** (147 mg, 0.25 mmol). [Cu(**4**)(POP)][PF_6] was isolated as an orange solid (290 mg, 0.22 mmol, 87%). ^{1}H NMR (500 MHz, acetone-d_6) δ/ppm: 8.68 (d, J = 1.6 Hz, 2H, H^{A3}), 7.97 (m, 4H, H^{B3}), 7.77 (d, J = 1.6 Hz, 2H, H^{A5}), 7.75 (m, 4H, H^{B2}), 7.45 (m, 2H, H^{C5}), 7.35 (t, J = 7.3 Hz, 4H, H^{D4}), 7.32–7.28 (overlapping m, 4H, H^{C3+C4}), 7.22 (t, J = 7.7 Hz, 8H, H^{D3}), 7.17 (m, 8H, H^{D2}), 7.08 (m, 2H, H^{C6}), 2.41 (s, 6H, H^{a}). ^{13}C NMR (126 MHz, acetone-d_6) δ/ppm: 160.3 (C^{A6}), 159.3 (C^{C1}), 154.3 (C^{A2}), 150.8 (C^{A4}), 139.5 (C^{B3}), 137.5 (C^{B1}), 134.7 (C^{C3}), 134.2 (t, J_{PC} = 7.8 Hz, C^{D2}), 133.5 (C^{C5}), 132.9 (t, J_{PC} = 16.2 Hz, C^{D1}), 131.0 (C^{D4}), 130.4 (C^{B2}), 129.8 (t, J_{PC} = 4.6 Hz, C^{D3}), 126.4 (C^{C4}), 126.3 (C^{C2}), 124.7 (C^{A5}), 121.2 (C^{C6}), 119.2 (C^{A3}), 97.0 (C^{B4}), 27.1 (C^{a}). ^{31}P NMR (202 MHz, acetone-d_6) δ/ppm −13.5 (bra, FWHM = 133 Hz), −144.5 (septet, J_{PF} = 710 Hz, $[PF_6]^-$). ESI MS: m/z 1189.0 $[M - PF_6]^+$ (base peak, calc. 1189.1). UV-vis (CH_2Cl_2, 2.5 × 10^{-5} mol dm^{-3}): λ/nm (ε/dm^3 mol^{-1} cm^{-1}) 229 (57 000), 273 (50 000), 315sh (29 800), 387 (4900). Found: C 53.88, H 3.91, N 2.25; $C_{60}H_{46}CuF_6I_2N_2OP_3$ requires C 53.97, H 3.74, N 2.10%.

[Cu(4)(xantphos)][PF$_6$]. [Cu(**4**)(xantphos)][PF_6] was prepared in an analogous manner to [Cu(**2**)(xantphos)][PF_6] using [Cu(MeCN)$_4$][PF_6] (93 mg, 0.25 mmol), xantphos (148 mg, 0.25 mmol) and **4** (147 mg, 0.25 mmol). The crude material was dissolved in a small amount of acetone, layered with Et_2O and left for two days. The resulting crystals were ground to a powder and dried under vacuum. [Cu(**4**)(xantphos)][PF_6] was isolated as an orange-red solid (138 mg, 0.10 mmol, 40%). ^{1}H NMR (500 MHz, acetone-d_6) δ/ppm: 8.60 (d, J = 1.7 Hz, 2H, H^{A3}), 7.96 (m, 4H, H^{B3}), 7.85 (dd, J = 7.8 Hz, J = 1.4 Hz, 2H, H^{C5}), 7.73 (d, J = 1.6 Hz, 2H, H^{A5}), 7.71 (m, 4H, H^{B2}), 7.41 (m, 4H, H^{D4}), 7.33 (t, J = 7.7 Hz, 2H, H^{C4}), 7.26–7.20 (overlapping m, 16H, H^{D2+D3}), 7.01 (m, 2H, H^{C3}), 2.23 (s, 6H, H^{a}), 1.77 (s, 6H, H^{b}). ^{13}C NMR (126 MHz, acetone-d_6) δ/ppm: 159.6 (C^{A6}), 153.9 (C^{A2}), 150.5 (C^{A4}), 139.3 (C^{B3}), 137.2 (C^{B1}), 134.8 (C^{C6}), 134.1 (t, J_{PC} = 7.7 Hz, C^{D2}), 132.5 (t, J_{PC} = 16.2 Hz, C^{D1}), 131.2 (C^{C3}), 131.1 (C^{D4}), 130.2 (C^{B2}), 129.8 (t, J_{PC} = 4.5 Hz, C^{D3}), 128.8 (C^{C5}), 126.4 (C^{C4}), 124.1 (C^{A5}), 122.6 (C^{C2}), 119.0 (C^{A3}), 96.8 (C^{B4}), 36.9 (C^{Cq}), 28.8 (C^{b}), 27.1 (C^{a}). ^{31}P NMR (202 MHz, acetone-d_6) δ/ppm −13.6 (broad, FWHM = 160 Hz), −144.5 (septet, J_{PF} = 710 Hz, $[PF_6]^-$). ESI MS: m/z 1229.1 $[M - PF_6]^+$ (base peak, calc. 1229.1). UV-vis (CH_2Cl_2, 2.5 × 10^{-5} mol dm^{-3}): λ/nm (ε/dm^3 mol^{-1} cm^{-1}) 230 (54 000), 278 (57 000), 316sh (29 100), 393 (5400). Found: C 55.02, H 3.92, N 2.27; $C_{63}H_{50}CuF_6I_2N_2OP_3$ requires C 55.02, H 4.62, N 2.04%.

[Cu(5)(POP)][PF$_6$]. [Cu(MeCN)$_4$][PF_6] (93.2 mg, 0.25 mmol) and POP (135 mg, 0.25 mmol) were dissolved in CH_2Cl_2 (30 ml) and the mixture was stirred for 1.5 h at room temperature. Compound **5** (84.1 mg, 0.25 mmol) was added and the mixture turned orange as it was stirred for another 2 h. Additional POP (26.9 mg, 0.05 mmol) was added; stirring was continued for another 1 h during which the solution turned yellow. After filtration, the solvent was removed from the filtrate; the solid residue was washed with hexane (2 × 30 ml) and Et_2O (7 × 30 ml) and dried under vacuum to give [Cu(**3**)(POP)][PF_6] (130 mg, 0.12 mmol, 48%) as a yellow solid. ^{1}H NMR (500 MHz, acetone-d_6) δ/ppm: 8.71 (d, J = 1.7 Hz, 2H, H^{A3}), 7.95 (m, 4H, H^{B2}), 7.76 (d, J = 1.6 Hz, 2H, H^{A5}), 7.61–7.54 (overlapping m, 6H, H^{B3+B4}), 7.45 (m, 2H, H^{C5}), 7.35 (m, 4H, H^{D4}), 7.32–7.27 (overlapping m, 4H, H^{C3+C4}), 7.25–7.16 (overlapping m, 16H, H^{D2+D3}), 7.08 (m, 2H, H^{C6}), 2.41 (s, 6H, H^{a}). ^{13}C NMR (126 MHz, acetone-d_6) δ/ppm: 159.9 (C^{A6}), 159.1 (C^{C1}), 154.2 (C^{A2}), 151.8 (C^{A4}), 137.7 (C^{B1}) 134.6 (C^{C3}), 134.0 (t, J_{PC} = 7.8 Hz, C^{D2}), 133.3 (C^{C5}), 132.9 (t, J_{PC} = 16.2 Hz, C^{D1}), 130.9 (overlapping m, C^{B4+D4}), 130.2 (C^{B3}), 129.6 (t, J_{PC} = 4.6 Hz, C^{D3}), 128.3 (C^{B2}), 126.2 (overlapping m, C^{C2+C4}), 124.7 (C^{A5}), 121.1 (C^{C6}), 119.2 (C^{A3}), 27.0 (C^{a}). ^{31}P NMR (202 MHz, acetone-d_6) δ/ppm −13.6 (broad, FWHM = 150 Hz), −144.5 (septet, J_{PF} = 707 Hz, $[PF_6]^-$). ESI MS: m/z 937.1 $[M - PF_6]^+$ (base peak, calc. 937.2). UV-vis (CH_2Cl_2, 2.5 × 10^{-5} mol dm^{-3}): λ/nm (ε/dm^3 mol^{-1} cm^{-1}) 230 (60 000), 264 (56 000), 312sh (24 000), 327sh (18 000), 387 (5100). Found: C 66.48, H 4.82, N 2.59; $C_{60}H_4CuF_6N_2OP_3$ requires C 66.51, H 4.47, N 2.59%.

[Cu(5)(xantphos)][PF$_6$]. [Cu(**5**)(xantphos)][PF_6] was prepared in the same manner as [Cu(**2**)(xantphos)][PF_6] starting with [Cu(MeCN)$_4$][PF_6] (93 mg, 0.25 mmol), xantphos (148 mg, 0.25 mmol) and **5** (84.1 mg, 0.25 mmol). [Cu(**5**)(xantphos)][PF_6] was isolated as a yellow solid (264 mg, 0.24 mmol, 94%). ^{1}H NMR (500 MHz, acetone-d$_6$) δ/ppm: 8.63 (d, J = 1.6 Hz, 2H, H^{A3}), 7.91 (m, 4H, H^{B2}), 7.85 (dd, J = 7.8 Hz, J = 1.4 Hz, 2H, H^{C5}), 7.72 (d, J = 1.5 Hz, 2H, H^{A5}), 7.60–7.53 (overlapping m, 6H, H^{B3+B4}), 7.41 (m, 4H, H^{D4}), 7.33 (t, J = 7.7 Hz, 2H, H^{C4}), 7.26–7.20 (overlapping m, 16H, H^{D2+D3}), 7.01 (m, 2H, H^{C3}), 2.24 (s, 6H, H^{a}), 1.77 (s, 6H, H^{b}). ^{13}C NMR (126 MHz, acetone-d_6) δ/ppm: 159.4 (C^{A6}), 155.9 (m, C^{C1}), 153.9 (C^{A2}), 151.7 (C^{A4}), 137.1 (C^{B1}), 134.9 (C^{C6}), 134.1 (t, J_{PC} = 7.7 Hz, C^{D2}), 132.6 (t, J_{PC} = 16.2 Hz, C^{D1}), 131.2 (C^{C3}), 131.0 (C^{D4}), 130.8 (C^{B4}), 130.1 (C^{B3}), 129.8 (t, J_{PC} = 4.5 Hz, C^{D3}), 128.9 (C^{C5}), 128.3 (C^{B2}), 126.4 (t, J_{PC} = 2.3 Hz, C^{C4}), 124.3 (C^{A5}), 122.7 (C^{C2}), 119.1 (C^{A3}), 36.9 (C^{Cq}), 28.7 (C^{b}), 27.1 (C^{a}). ^{31}P NMR (202 MHz, acetone-d_6) δ/ppm −13.5 (broad, FWHM = 180 Hz), −144.2 (septet, J_{PF} = 708 Hz, $[PF_6]^-$). ESI MS: m/z 977.2 $[M - PF_6]^+$ (base peak, calc. 977.3). UV-vis (CH_2Cl_2, 2.5 × 10^{-5} mol dm^{-3}): λ/nm (ε/dm^3 mol^{-1} cm^{-1}) 231 (59 000), 266 (55 000), 312sh (20 000), 326sh (17 000), 389 (4800). Found: C 67.05, H 5.00, N 2.67; $C_{63}H_{52}CuF_6N_2OP_3$ requires C 67.35, H 4.67, N 2.49%.

Crystallography

Data were collected on a Bruker Kappa Apex2 diffractometer with data reduction, solution and refinement using the programs APEX[49] and CRYSTALS.[50] Structural analysis was carried out using Mercury v. 3.7.[51,52]

[Cu(1)(POP)][PF$_6$]·0.8H$_2$O. $C_{60}H_{48.6}CuF_8N_2O_{1.8}P_3$, M = 1134.91, yellow block, triclinic, space group $P\bar{1}$, a = 11.8717(7), b = 14.5153(11), c = 17.3347(11) Å, α = 76.797(5), β = 84.595(4), γ = 88.547(4)°, U = 2895.2(3) Å^3, Z = 2, D_c = 1.302 Mg m^{-3}, μ(CuKα) = 1.894 mm^{-1}, T = 123 K. Total 36 247 reflections, 10 430 unique, R_{int} = 0.060. Refinement of 5821 reflections (828 parameters) with $I > 2\sigma(I)$ converged at final R_1 = 0.1078 (R_1 all data = 0.1526), wR_2 = 0.2856 (wR_2 all data = 0.3329), gof = 1.0746. CCDC 1486908.

[Cu(1)(xantphos)][PF$_6$]·Et$_2$O. $C_{67}H_{60}CuF_8N_2O_2P_3$, M = 1233.68, yellow block, monoclinic, space group $P2_1/c$, a = 14.3066(14), b = 16.4396(16), c = 25.643(3) Å, β = 101.190(3)°, U = 5916.4(10) Å^3, Z = 4, D_c = 1.385 Mg m^{-3}, μ(Cu-Kα) = 1.901 mm^{-1}, T = 123 K. Total 92 310 reflections, 10 709 unique, R_{int} = 0.027. Refinement of 10 362 reflections (748 parameters) with $I > 2\sigma(I)$ converged at final R_1 = 0.0573 (R_1 all data = 0.0644), wR_2 = 0.1114 (wR_2 all data = 0.1149), gof = 0.7666. CCDC 1486909.

[Cu(3)(xantphos)][PF$_6$]·0.5H$_2$O·Et$_2$O. $C_{67}H_{61}Br_2CuF_6N_2O_{2.5}P_3$, M = 1233.68, yellow block, triclinic, space group $P\bar{1}$, a = 10.8614(6), b = 17.1071(8), c = 18.6668(9) Å, α = 76.277(3), β = 85.698(3), γ = 77.922(3)°, U = 3293.7(3) Å^3, Z = 2, D_c = 1.376 Mg m^{-3}, μ(CuKα) = 3.089 mm^{-1}, T = 123 K. Total 40 048 reflections, 11 720 unique, R_{int} = 0.082. Refinement of 11 716 reflections (845 parameters) with $I > 2\sigma(I)$ converged at final R_1 = 0.1035 (R_1 all data = 0.1727), wR_2 = 0.2563 (wR_2 all data = 0.3243), gof = 0.9690. CCDC 1486906.

[Cu(4)(xantphos)][PF$_6$]·2Et$_2$O. $C_{71}H_{70}CuF_6I_2N_2O_3P_3$, M = 1523.61, yellow plate, triclinic, space group $P\bar{1}$, a = 10.8361(6), b = 16.8690(10), c = 19.1696(11) Å, α = 74.934(2), β = 88.594(2), γ = 79.074(2)°, U = 3321.2(3) Å^3, Z = 2, D_c = 1.523 Mg m^{-3}, μ(CuKα) = 8.984 mm^{-1}, T = 123 K. Total 35 841 reflections, 12 100 unique, R_{int} = 0.026. Refinement of 11 776 reflections (793 parameters) with $I > 2\sigma(I)$ converged at final R_1 = 0.0455 (R_1 all data = 0.0466), wR_2 = 0.0948 (wR_2 all data = 0.0949), gof = 0.8865. CCDC 1486907.

[Cu(5)(xantphos)][PF$_6$]. $C_{63}H_{52}CuF_6N_2OP_3$, M = 1123.57, yellow plate, hexagonal, space group $P6_1$, $a = b$ = 10.9508(5), c = 76.094(3) Å, U = 7902.6(7) Å^3, Z = 6, D_c = 1.416 Mg m^{-3}, μ(Cu-Kα) = 2.008 mm^{-1}, T = 123 K. Total 30 411 reflections, 8703 unique, R_{int} = 0.028. Refinement of 8359 reflections (686 parameters) with $I > 2\sigma(I)$ converged at final R_1 = 0.0311 (R_1 all data = 0.0330), wR_2 = 0.0674 (wR_2 all data = 0.0679), gof = 0.9999. CCDC 1486911.

[Cu(1)$_2$][PF$_6$]. $C_{48}H_{36}CuF_{10}N_4P$, M = 953.33, orange block, monoclinic, space group $C2/c$, a = 24.1972(18), b = 16.3688(12), c = 23.0149(19) Å, β = 108.421(4)°, U = 8648.6(12) Å^3, Z = 8, D_c = 1.464 Mg m^{-3}, μ(CuKα) = 1.791 mm^{-1}, T = 123 K. Total 30 204 reflections, 7813 unique, R_{int} = 0.043. Refinement of 6016 reflections (580 parameters) with $I > 2\sigma(I)$ converged at final R_1 = 0.0594 (R_1 all data = 0.0791), wR_2 = 0.1303 (wR_2 all data = 0.1398), gof = 1.0319. CCDC 1486910.

Device preparation

LECs were prepared on pre-patterned indium tin oxide (ITO) covered glass substrates. The substrates were previously cleaned using subsequent sonication with soap, deionized water and 2-propanol. After drying with a N_2 flow, the substrates were placed in a UV Ozone cleaner (Jelight 42-220) for 20 minutes. An Ambios XP-1 profilometer was used to determine the layer thickness. Following, 80 nm of poly(3,4-ethylenedioxythiophene):poly(styrenesulfonate) (PEDOT:PSS) (CLEVIOS™ P VP AI 4083, aqueous dispersion, 1.3–1.7% solid content, Heraeus) was coated in order to avoid the formation of pinholes and to improve the reproducibility of the cells. Subsequently, the emitting layer was deposited by spin-coating from a 2-butanone solution of the emitting compound with the addition of the ionic liquid 1-ethyl-3-methylimidazolium hexafluoridophosphate [Emim][PF$_6$] (>98.5%, Sigma-Aldrich) in a 4 to 1 molar ratio. The active layer spin conditions were optimized to form 100 nm thick films. 70 nm of aluminium, acting as the top electrode, were thermally evaporated onto the device using an Edwards Auto500 evaporator integrated into an inert atmosphere glovebox (<0.1 ppm O_2 and H_2O, MBraun). The active areas of the devices are 6.5 mm^2. The devices were then characterized under inert atmosphere conditions at room temperature.

Device characterization

The devices were measured by applying a pulsed current (J = 50 A m^{-2}, 1 kHz, 50% duty cycle) and monitoring the voltage and luminance *versus* time by using a True Colour Sensor MAZeT (MTCSiCT sensor) with a Botest OLT OLED Lifetime-Test system. The electroluminescence (EL) spectra were measured using an Avantes AvaSpec-2048 fiber optic spectrometer during device measurements. The turn-on time (t_{max}) is defined as the time to reach the maximum luminance (Lum_{max}) and the lifetime ($t_{1/2}$) is the time to reach one-half of Lum_{max} after this value is attained.

Results and discussion

Synthesis and characterization of the [Cu(N^N)(P^P)][PF$_6$] complexes

The formation of homoleptic [Cu(N^N)$_2$]$^+$, [Cu(P^P)$_2$]$^+$ and [Cu(P^P)]$^+$ may compete with that of the desired heteroleptic [Cu(N^N)(P^P)]$^+$ species from the reaction of [Cu(MeCN)$_4$][PF$_6$] with the respective N^N and P^P ligands.[35,53] The POP ligand is more sterically demanding than xantphos, as demonstrated by Kawai and coworkers who showed that the reaction of [Cu(MeCN)$_4$]$^+$ with one equivalent of POP or xantphos leads to [Cu(POP)(NCMe)]$^+$ or [Cu(xantphos)(NCMe)$_2$]$^+$, respectively, while with two equivalents, the products are [Cu(POP-*P*,*P*′)(POP-*P*)]$^+$ or [Cu(xantphos-*P*,*P*′)$_2$]$^+$.[54] This leads to different optimal strategies[22–24] for preparing [Cu(N^N)(POP)][PF$_6$] and [Cu(N^N)(xantphos)][PF$_6$]. The [Cu(N^N)(POP)][PF$_6$] (N^N = **1–5**) complexes were synthesized in a stepwise manner, first combining POP and [Cu(MeCN)$_4$][PF$_6$] in CH_2Cl_2 and then, after 2 hours, adding the N^N ligand to the reaction mixture. The [Cu(N^N)(xantphos)][PF$_6$] complexes were obtained by addition of a CH_2Cl_2 solution containing N^N and xantphos (1 : 1) to a

CH_2Cl_2 solution of $[Cu(MeCN)_4][PF_6]$. In the initial stages of the reaction, a red colour is observed indicating the presence of $[Cu(N^N)_2]^+$, but over time the yellow or bright orange colour of the heteroleptic complex develops. NMR spectra of CD_2Cl_2 solutions of some of the $[Cu(N^N)(P^P)][PF_6]$ complexes showed the presence of both homo- and heteroleptic complexes; in contrast, the heteroleptic complexes were stable in acetone-d_6. The isolation of single crystals of $[Cu(\mathbf{1})_2][PF_6]$ from a CH_2Cl_2 solution initially containing $[Cu(\mathbf{1})(POP)][PF_6]$ (see later) also demonstrates that ligand redistribution can occur in CH_2Cl_2.

The complexes $[Cu(N^N)(POP)][PF_6]$ and $[Cu(N^N)(xantphos)][PF_6]$ were isolated as yellow or orange solids in yields ranging from 40 to 98%. The electrospray mass spectrum of each complex showed a peak envelope (base peak) corresponding to $[M - PF_6]^+$, and ^1H and ^{13}C NMR spectra were consistent with the presence of both N^N and P^P ligands. The ^{31}P NMR spectrum of each complex showed the $[PF_6]^-$ ion (δ −144.5 ppm) and a broad signal (δ −13.3 to −13.6 ppm, see the Experimental section for FWHM) assigned to the coordinated POP or xantphos ligand. The solution ^1H NMR spectra of $[Cu(\mathbf{5})(POP)][PF_6]$ and $[Cu(\mathbf{5})(xantphos)][PF_6]$ are shown as representative examples in Fig. 1; atom numbering is shown in Scheme 2. Spectra were assigned using COSY, NOESY, HMQC and HMBC techniques. On going from $[Cu(\mathbf{5})(POP)]^+$ (Fig. 1a) to $[Cu(\mathbf{5})(xantphos)]^+$ (Fig. 1b), the noteworthy change in the ^1H NMR spectrum is the loss of the signal for H^{C6} as the CMe_2 bridge is introduced into the P^P ligand. The methyl groups in ligand **5** give rise to a signal at δ 2.41 ppm in $[Cu(\mathbf{5})(POP)]^+$ and δ 2.24 ppm in $[Cu(\mathbf{5})(xantphos)]^+$; the CMe_2 group in the latter is characterized by a singlet at δ 1.77 ppm.

Fig. 2 compares the solution ^1H NMR spectra of the $[Cu(N^N)(xantphos)][PF_6]$ complexes. As expected, the resonances for the xantphos ligand are not affected by the remote halo-substituents in the diimine ligands. The only significant changes involve signals for protons H^{B2} and H^{B3} (see Scheme 2), and the trend mimics that observed in the series of

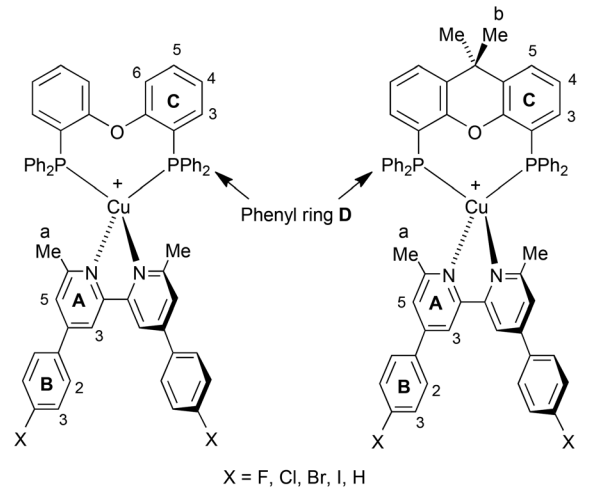

Scheme 2 Atom numbering for NMR assignments in $[Cu(N^N)(POP)]^+$ and $[Cu(N^N)(xantphos)]^+$ (N^N = **1–5**).

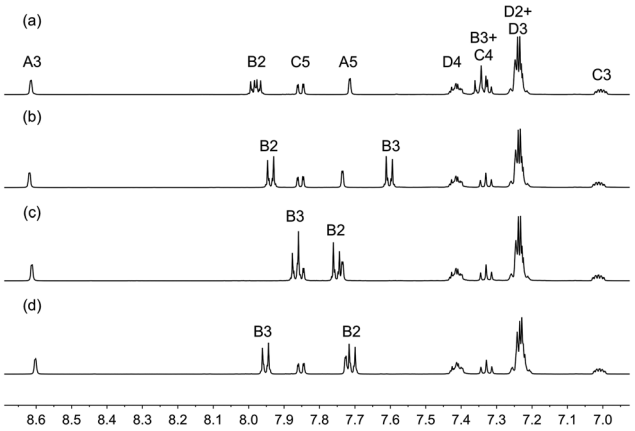

Fig. 2 The aromatic regions of the ^1H NMR (500 MHz, 298 K, acetone-d_6) of (a) $[Cu(\mathbf{1})(xantphos)][PF_6]$, (b) $[Cu(\mathbf{2})(xantphos)][PF_6]$, (c) $[Cu(\mathbf{3})(xantphos)][PF_6]$ and (d) $[Cu(\mathbf{4})(xantphos)][PF_6]$. Chemical shifts in δ/ppm. See Scheme 2 for labelling.

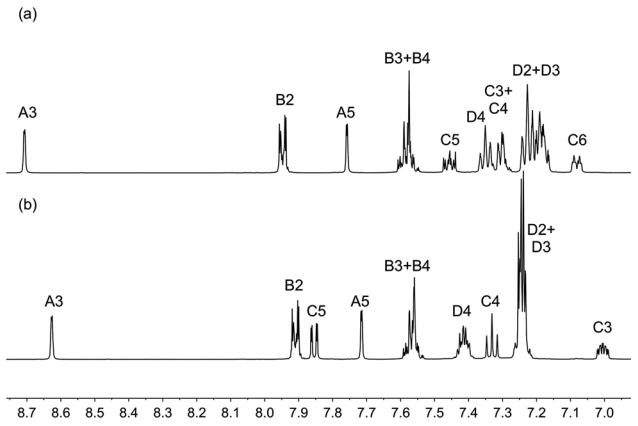

Fig. 1 The aromatic regions of the ^1H NMR spectra (500 MHz, 298 K, acetone-d_6) of (a) $[Cu(\mathbf{5})(POP)][PF_6]$ and (b) $[Cu(\mathbf{5})(xantphos)][PF_6]$. Chemical shifts in δ/ppm. See Scheme 2 for labelling.

homoleptic complexes $[Cu(\mathbf{1})_2][PF_6]$, $[Cu(\mathbf{2})_2][PF_6]$ $[Cu(\mathbf{3})_2][PF_6]$ and $[Cu(\mathbf{4})_2][PF_6]$.[45]

Single crystals of $[Cu(\mathbf{1})(xantphos)][PF_6]\cdot Et_2O$, $[Cu(\mathbf{3})(xantphos)][PF_6]\cdot 0.5H_2O\cdot Et_2O$, $[Cu(\mathbf{4})(xantphos)][PF_6]\cdot 2Et_2O$ and $[Cu(\mathbf{5})(xantphos)][PF_6]$ were grown by layering a CH_2Cl_2 solution of the compound with Et_2O. The quality of the structure of $[Cu(\mathbf{3})(xantphos)][PF_6]\cdot 0.5H_2O\cdot Et_2O$ was poor due to weakly diffracting crystals, and persistent attempts to grow better quality crystals were unsuccessful. We therefore refrain from detailed discussion of this structure. $[Cu(\mathbf{3})(xantphos)][PF_6]\cdot 0.5H_2O\cdot Et_2O$ (Fig. S1†) and $[Cu(\mathbf{4})(xantphos)][PF_6]\cdot 2Et_2O$ both crystallize in the triclinic space group $P\bar{1}$ and are structurally similar. $[Cu(\mathbf{1})(xantphos)][PF_6]\cdot Et_2O$ crystallizes in the monoclinic space group $P2_1/c$ and $[Cu(\mathbf{5})(xantphos)][PF_6]$ in the hexagonal space group $P6_1$; the latter is one of the 65 Sohncke space groups

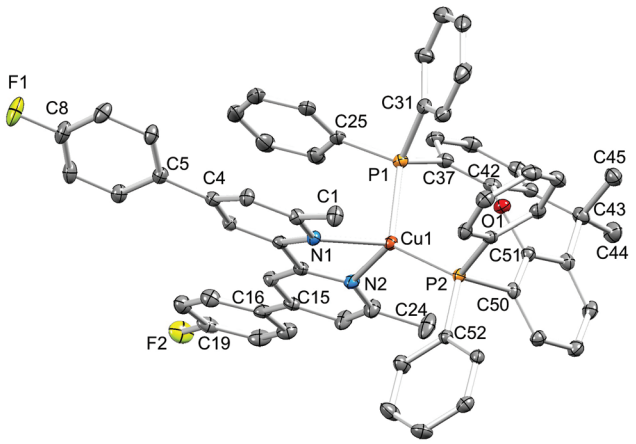

Fig. 3 Structure of the $[Cu(\mathbf{1})(xantphos)]^+$ cation in $[Cu(\mathbf{1})(xantphos)][PF_6]\cdot Et_2O$ with ellipsoids plotted at the 40% probability level; H atoms are omitted for clarity. Selected bond parameters: Cu1–P2 = 2.2470(8), Cu1–P1 = 2.3159(8), Cu1–N1 = 2.084(2), Cu1–N2 = 2.102(2) Å; P2–Cu1–P1 = 117.09(3), P2–Cu1–N1 = 128.64(6), P1–Cu1–N1 = 99.52(6), P2–Cu1–N2 = 124.20(6), P1–Cu1–N2 = 100.98(7), N1–Cu1–N2 = 77.73(9)°.

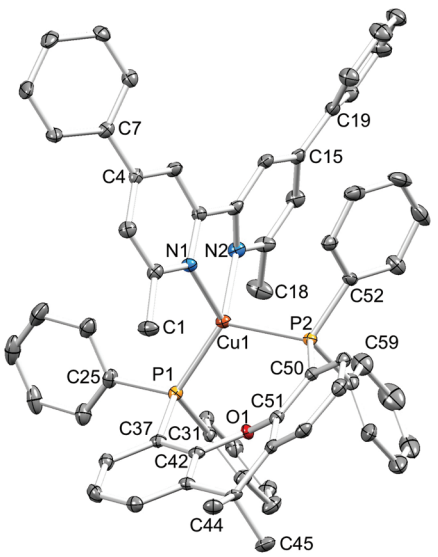

Fig. 5 Structure of the $[Cu(\mathbf{5})(xantphos)]^+$ cation in $[Cu(\mathbf{5})(xantphos)][PF_6]$ with ellipsoids plotted at the 40% probability level; H atoms are omitted for clarity. Selected bond parameters: Cu1–P2 = 2.3100(7), Cu1–P1 = 2.2614(7), Cu1–N2 = 2.132(2), Cu1–N1 = 2.090(2) Å; P2–Cu1–P1 = 115.83(3), P2–Cu1–N2 = 100.19(6), P1–Cu1–N2 = 125.23(6), P2–Cu1–N1 = 108.59(6), P1–Cu1–N1 = 120.93(6), N2–Cu–N1 = 79.74(8)°.

(see below). Fig. 3–5 show the structures of the $[Cu(\mathbf{1})(xantphos)]^+$, $[Cu(\mathbf{4})(xantphos)]^+$ and $[Cu(\mathbf{5})(xantphos)]^+$ cations. In each, atom Cu1 is in a distorted tetrahedral coordination environment, with Cu–P and Cu–N bond lengths in typical ranges (see captions to Fig. 3–5); halo-substitution does not have a significant impact on the coordination environment at copper. In each cation, the pyran ring adopts a boat conformation, consistent with crystallographic data for related structures.[22,55]

In the $[Cu(\mathbf{1})(xantphos)]^+$ and $[Cu(\mathbf{4})(xantphos)]^+$ cations, the bpy unit is close to planar (angles between the pyridine-ring planes = 5.0° and 2.5°, respectively). In contrast, the bpy unit is significantly twisted in $[Cu(\mathbf{5})(xantphos)]^+$ (angle between ring planes = 31.6°). In $[Cu(\mathbf{1})(xantphos)][PF_6]$, the fluorophenyl substituent containing F2 is approximately coplanar (twist angle = 7.8°) with the pyridine ring (with N1) to which it is bonded. This planarity is associated with the presence of triple-decker π-stacks between centrosymmetric pairs of $[Cu(\mathbf{1})(xantphos)]^+$ cations (Fig. 6a). These involve the aromatic rings containing C25 (phenyl of xantphos), N1 and $C19^i$ (fluorophenyl ring, $i = -x, 1-y, 1-z$); in the triple-decker π-stack, the ring–centroid separations are 3.39 and 3.44 Å, and the centroid–centroid distances are 3.72 and 3.61 Å. In contrast, in the iodo-derivative $[Cu(\mathbf{4})(xantphos)][PF_6]$, centrosymmetric pairs of cations interact through π-stacking of the iodophenyl rings (Fig. 6b); the distance between the ring-

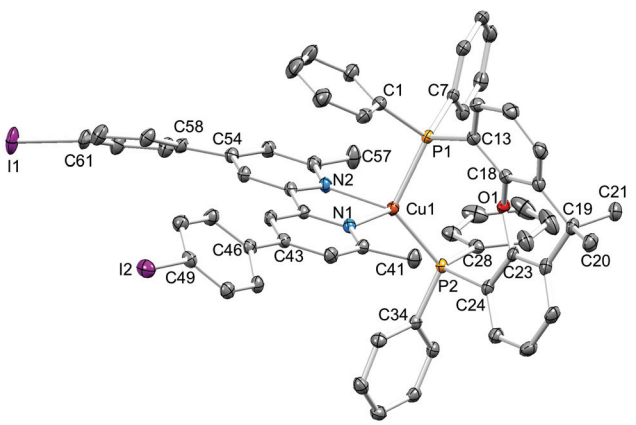

Fig. 4 Structure of the $[Cu(\mathbf{4})(xantphos)]^+$ cation in $[Cu(\mathbf{4})(xantphos)][PF_6]\cdot 2Et_2O$ with ellipsoids plotted at the 40% probability level; H atoms are omitted for clarity. Selected bond parameters: Cu1–P1 = 2.3138(9), Cu1–P2 = 2.2717(9), Cu1–N1 = 2.077(3), Cu1–N2 = 2.135(3) Å; P1–Cu1–P2 = 116.90(3), P1–Cu1–N1 = 104.53(7), P2–Cu1–N1 = 117.77(8), P1–Cu1–N2 = 101.52(8), P2–Cu1–N2 = 129.47(8), N1–Cu1–N2 = 79.18(10)°.

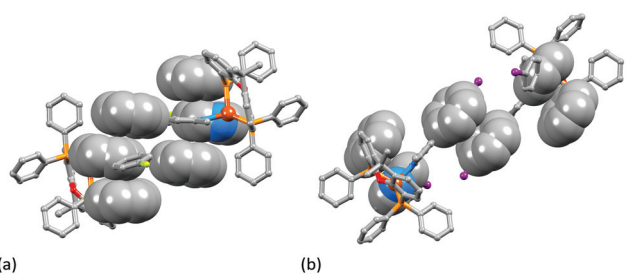

Fig. 6 (a) Packing of centrosymmetric pairs of $[Cu(\mathbf{1})(xantphos)]^+$ cations with intra/intermolecular triple-decker π-stacks. (b) Intramolecular π-stacking in $[Cu(\mathbf{4})(xantphos)]^+$ cations, and interactions between centrosymmetric pairs of cations.

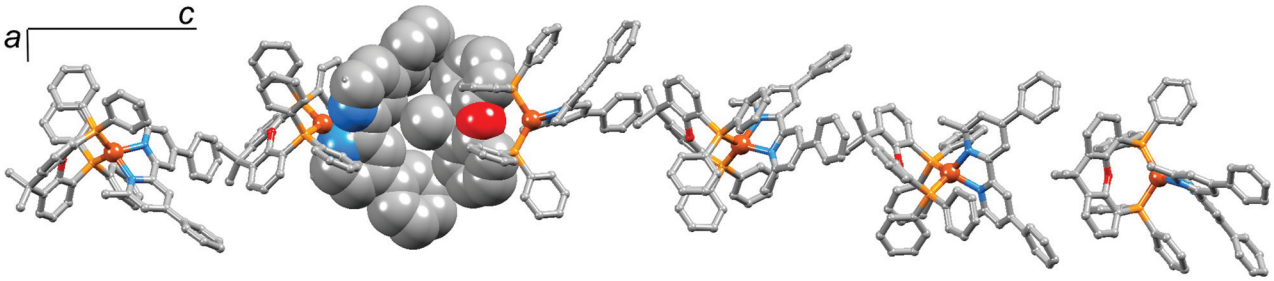

Fig. 7 Arrangement of [Cu(**5**)(xantphos)]$^+$ cations along the 6-fold screw axis; the accommodation of the xantphos domain within the cavity created by the twisted 4,4′-diphenylbpy unit of a neighbouring cation is shown in space-filling representation.

planes and the inter-centroid separation are, respectively, 3.32 and 3.70 Å. Each [Cu(**4**)(xantphos)]$^+$ cation also exhibits an intramolecular π-stacking interaction between one phenyl ring of xantphos and a pyridine ring (Fig. 6b).

We noted above that in [Cu(**5**)(xantphos)][PF_6], the dihedral angle between the pyridine rings in **5** is 31.6°. The twisting of the 4,4′-diphenylbpy unit is a consequence of the chiral arrangement along the 6-fold screw axis which follows the *c*-axis (Fig. 7). The twisted 4,4′-diphenylbpy domain forms a cavity which accommodates the xantphos unit of an adjacent cation (Fig. 7), leading to highly efficient packing of cations in infinite chains.

Yellow, single crystals of [Cu(**1**)(POP)][PF_6]·0.8H_2O were obtained from a CH_2Cl_2 solution of [Cu(**1**)(POP)][PF_6] layered with Et_2O. However, whilst these crystals grew, orange crystals of [Cu(**1**)$_2$][PF_6] also formed (see earlier discussion on ligand lability). Structure quality for [Cu(**1**)(POP)][PF_6]·0.8H_2O was poor due to weakly diffracting crystals (especially at high angles), but provided confirmation of the gross structural details of the heteroleptic complex (Fig. S2†). [Cu(**1**)$_2$][PF_6] crystallizes in the monoclinic space group *C*2/*c*, and the structure of the [Cu(**1**)$_2$]$^+$ cation and bond parameters for the copper coordination sphere are given in Fig. S3.† The structure of the cation is similar to that of the dibromo analogue in 2{[Cu(**3**)$_2$][PF_6]}·3Me_2CO;[56] Cu–N bond lengths are unexceptional (range 2.000(2) to 2.044(2) Å). The angle between the least squares planes containing Cu1 and each (near planar) bpy unit is 88.0°, very close to the 85.6° observed in [Cu(**3**)$_2$]$^+$.[56] The tetrahedral coordination environment in both these [Cu(N^N)$_2$]$^+$ cations is therefore less flattened than in the salts of [Cu(6,6′-Me_2bpy)$_2$]$^+$ (range = 74.3 to 80.9°).[57]

Electrochemistry

The electrochemical behaviour of the [Cu(N^N)(P^P)][PF_6] complexes was investigated using cyclic voltammetry and data are given in Table 1 and a typical CV is shown in Fig. 8. The single oxidation wave for each complex is attributed to the copper-centred oxidation process. For the POP-containing complexes, this process is irreversible whilst with xantphos, it is quasi-reversible provided that the potentials do not rise above ~+1.1 V (Fig. 8). The presence of the halo-substituents has a negligible effect on $E^{ox}_{1/2}$. The values of $E^{ox}_{1/2}$ ~ +0.9 V are compared with +0.82 and +0.81 V for [Cu(6,6′-Me_2bpy)(POP)][BF_4] and [Cu(6,6′-Me_2bpy)(xantphos)][BF_4] (MeCN solution, *vs.* Fc/Fc$^+$).[33] Reduction processes were poorly defined within the solvent accessible window.

Table 1 Cyclic voltammetric data for [Cu(N^N)(P^P)][PF_6] complexes referenced to internal Fc/Fc$^+$ = 0. V; CH_2Cl_2 (freshly distilled or degassed HPLC grade) solutions with [^{n}Bu$_4$N][PF_6] as the supporting electrolyte and a scan rate of 0.1 V s^{-1}. Processes are quasi-reversible unless otherwise stated (ir = irreversible)

Complex cation	$E^{ox}_{1/2}$/V ($E_{pc} - E_{pa}$/mV)	E_{pc}/V
[Cu(**1**)(POP)]$^+$		+0.99^{ir}
[Cu(**2**)(POP)]$^+$		+0.99^{ir}
[Cu(**3**)(POP)]$^+$		+0.98^{ir}
[Cu(**4**)(POP)]$^+$		+0.99^{ir}
[Cu(**5**)(POP)]$^+$		+0.95^{ir}
[Cu(**1**)(xantphos)]$^+$	+0.91 (144)	
[Cu(**2**)(xantphos)]$^+$	+0.92 (133)	
[Cu(**3**)(xantphos)]$^+$	+0.92 (141)	
[Cu(**4**)(xantphos)]$^+$	+0.91 (119)	
[Cu(**5**)(xantphos)]$^+$	+0.88 (123)	

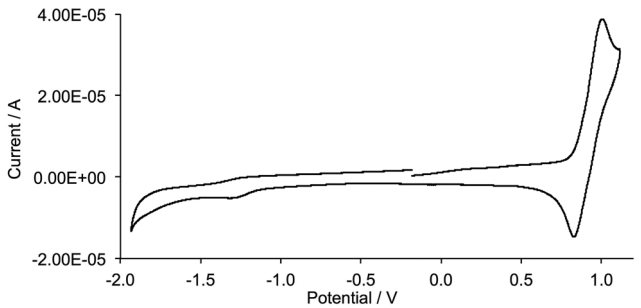

Fig. 8 Cyclic voltammogram for a CH_2Cl_2 solution of [Cu(**3**)(xantphos)][PF_6]; scan rate 0.1 V s^{-1} and referenced internally to Fc/Fc$^+$.

Photophysical properties

Fig. 9 and S4† display the solution absorption spectra of the [Cu(N^N)(xantphos)][PF_6] and [Cu(N^N)(POP)][PF_6] complexes, respectively. The intense bands below ~330 nm arise from ligand-based π → π* and n → π* transitions. Introduction of the halo-substituents shifts the highest energy absorption

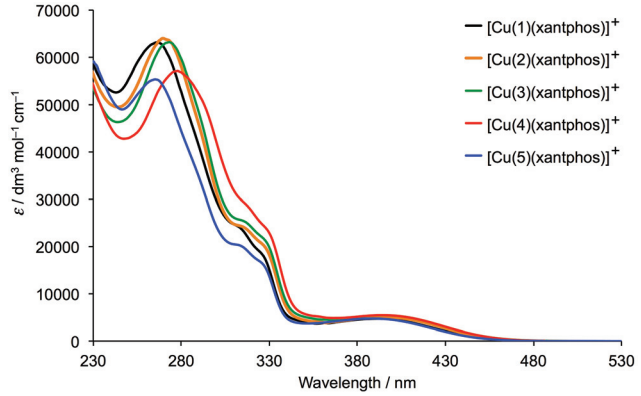

Fig. 9 Solution (CH_2Cl_2, 2.5 × 10^{-5} mol dm^{-3}) absorption spectra of [Cu(N^N)(xantphos)][PF_6] (N^N = **1–5**).

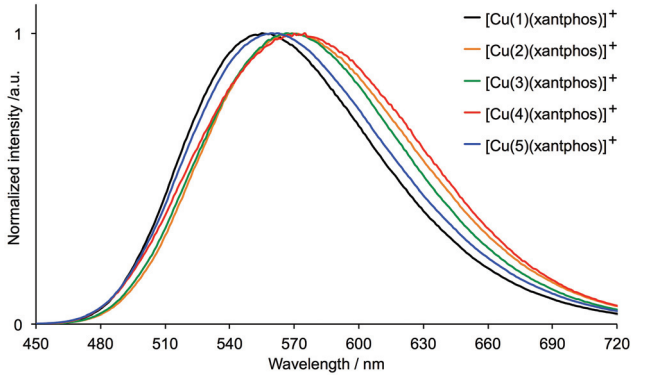

Fig. 11 Normalized solid-state emission spectra of [Cu(N^N)(xantphos)][PF_6] (N^N = **1–5**) (λ_{exc} = 365 nm).

maximum shown in Fig. 9 from 266 nm to 278 nm, the lowest energy being the complex containing the iodo-functionality. The same trend is observed for the [Cu(N^N)(POP)][PF_6] series (λ_{max} shifts from 266 to 278 nm, Fig. S4†) and reflects that observed for the free N^N ligands.[45] The broad absorption in the range 387–395 nm is attributed to metal-to-ligand charge transfer (MLCT).

The PL spectra of the solution, powder and thin film samples of [Cu(N^N)(POP)][PF_6] are shown in Fig. 10, S5 and S7,† and of [Cu(N^N)(xantphos)][PF_6] are displayed in Fig. S6, 11 and S8.† All complexes are yellow or yellow-orange emitters and Table 2 gives values of λ_{em}^{max} as well as PL quantum yields and emission lifetimes. The emission spectra are broad and generally structureless, although the solution spectra of [Cu(**3**)(POP)][PF_6] and [Cu(**3**)(xantphos)][PF_6] both exhibit a high energy shoulder (Fig. 10 and S6†). Little difference is observed in the solution spectra of any given pair of $[Cu(N^N)(POP)]^+$ and $[Cu(N^N)(xantphos)]^+$ complexes. The most blue-shifted spectra are for complexes with **5** (no halo-substituent) and the most red-shifted are for those in which N^N = **4** (iodo-functionalized). [Cu(**4**)(POP)][PF_6] is very weakly emissive (PLQY = 1% in the solid state). For the xantphos-containing compounds, [Cu(**4**)(xantphos)][PF_6] shows the lowest PLQY in the powder (Table 2). Complexes containing N^N ligands **1**, **2**, **3** or **5** undergo a blue shift on comparing the solution with the solid state (except for complexes with ligand **5** in thin film). This is consistent with other $[Cu(N^N)(POP)]^+$ emitters,[22,24,30] although the opposite trend has been observed when N^N = 2,2′:6′,2″-terpyridine.[58] The PLQY of degassed solutions of [Cu(N^N)(POP)][PF_6] are generally higher than that of the xantphos-containing analogues (Table 2). However, in the solid state, due to packing interactions, luminescence properties can be significantly influenced by the type of substituent; this is more prevalent in powders than in thin films. An explanation for this behaviour has previously been proposed on the basis of the flattening that the pseudo-tetragonal geometry of the complexes experience while passing from the electronic ground state (S_0) to the emitting excited state.[44] This flattening, which is more favoured in a fluid medium, is hindered in the crystalline state (powder) and is partially hindered in thin films. The highest PLQY values are exhibited by the fluoro-functionalized complexes; powdered [Cu(**1**)(POP)][PF_6] has a PLQY = 74% with a lifetime $\tau_{1/2}$ = 11.1 μs (Tables 2 and S1†), while the thin film has a PLQY = 13%. The range of values of $\tau_{1/2}$ (Table 2) is similar to that observed for [Cu(N^N)(POP)][PF_6] and [Cu(N^N)(xantphos)][PF_6] complexes in which N^N = 6-methyl-2,2′-bipyridine, 6-ethyl-2,2′-bipyridine, 6-phenyl-2,2′-bipyridine or 6,6′-dimethyl-2,2′-bipyridine,[22,24] and for [Cu(6,6′-Me_2bpy)(POP)][BF_4] in PMMA thin-films.[33] The solid-state emission data indicate that the introduction of the remote fluoro-substituent enhances PL (compare complexes with N^N = **1** *versus* **5**), but that replacement of the fluorine atom by a heavier congener in ligands **2**, **3** or **4** is detrimental.

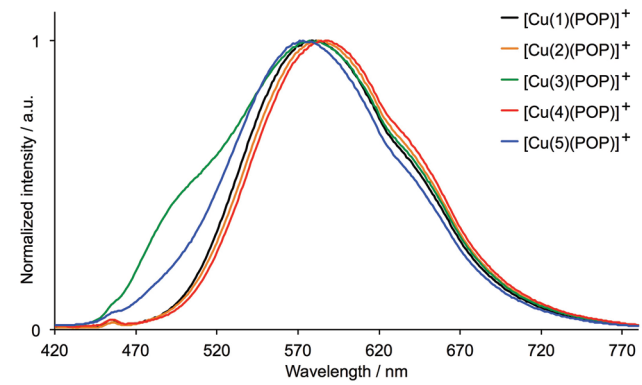

Fig. 10 Normalized solution (CH_2Cl_2, 2.5 × 10^{-5} mol dm^{-3}) emission spectra of [Cu(N^N)(POP)][PF_6] (λ_{exc} = 400 nm, see Table 2 for λ_{em}^{max}).

Electroluminescence

The electroluminescence behaviour of the complexes was tested by incorporating them into LEC devices. For LEC characterization, the turn-on time (t_{max}) is defined as the time to reach the maximum luminance (Lum_{max}). The time to reach one-half of the maximum luminance is referred to as $t_{1/2}$ (the device lifetime). The devices were operated using a block-wave

Table 2 Emission maxima, photoluminescence quantum yields (PLQY) and lifetimes ($\tau_{1/2}$) for [Cu(N^N)(P^P)][PF_6] complexes

	CH_2Cl_2 solution			Powder[b]			Thin film[b,d]	
Complex cation	λ_{em}^{max}/nm	PLQY[a,b] (non-degassed/degassed)/%	$\tau_{1/2}$(av)[a,b] (degassed)/μs	λ_{em}^{max}/nm	PLQY/%	$\tau_{1/2}$(av)[c]/μs	λ_{em}^{max}/nm	PLQY/%
[Cu(**1**)(POP)]$^+$	578	2/26	4.5	542	74	11.1	573	13
[Cu(**2**)(POP)]$^+$	583	2/21	4.3	567	12	4.0	571	4
[Cu(**3**)(POP)]$^+$	577	3/21	4.4	570	11	4.2	574	2
[Cu(**4**)(POP)]$^+$	589	1/14	4.1	590	1	1.2	580	1
[Cu(**5**)(POP)]$^+$	573	2/22	3.0[c]	550	44	10.2	576	8
[Cu(**1**)(xantphos)]$^+$	576	1/12	2.5	555	25	5.8	565	16
[Cu(**2**)(xantphos)]$^+$	577	2/12	2.8	569	18	5.2	572	11
[Cu(**3**)(xantphos)]$^+$	571	2/12	2.7	567	14	6.1	573	10
[Cu(**4**)(xantphos)]$^+$	579	2/12	2.6	575	8	3.0	576	6
[Cu(**5**)(xantphos)]$^+$	570	2/15	3.7	562	21	5.7	570	10

[a] Solution concentration = 2.5×10^{-5} mol dm^{-3} except for [Cu(**5**)(POP)][PF_6] (1.0×10^{-5} mol dm^{-3}) and [Cu(**5**)(xantphos)][PF_6] (1.88×10^{-5} mol dm^{-3}). [b] λ_{exc} = 365 nm. [c] Biexponential fit using the equation $\tau_{1/2}(av) = \sum A_i\tau_i / \sum A_i$ where A_i is the pre-exponential factor for the lifetime (see Table S1). [d] Thin films consisted of the [Cu(N^N)(P^P)][PF_6] complex mixed with the ionic liquid (IL) 1-ethyl-3-methylimidazolium hexafluoridophosphate in a molar ratio 4 : 1 (complex : IL).

pulsed current driving mode (as described in the Experimental section), which was selected in order to enhance the device response. Under these conditions, the voltage required to maintain the current density decreases *versus* time due to the formation of p- and n-doped regions, which reduces the resistance of the active layer. The electroluminescence (EL) spectra recorded for the LECs showed maxima in the 565–585 nm range (yellow emission) for all complexes (Fig. S9†).

On the one hand, LECs containing [Cu(**4**)(POP)]$^+$, [Cu(**4**)(xantphos)]$^+$ and [Cu(**3**)(POP)]$^+$, which contain the complexes with iodo- and bromo-substituted N^N ligands, did not show any EL after 50 hours (Fig. S10–S12†). However, the LEC with [Cu(**3**)(xantphos)]$^+$ (which also has a bromo-functionalized N^N) showed EL, although this is rather low. The device characteristics for this LEC are depicted in Fig. S13.† This LEC showed a fast t_{max} (10 s), although a rather low Lum_{max} of 10 cd m^{-2}. Moreover, the device exhibited a fast luminance decay, and hence a poor device lifetime ($t_{1/2}$ = 4.3 min). These results seem to indicate that the attached bromo or iodo atoms have a detrimental effect on the device performances. In view of the weak EL for one bromo-containing complex, it would appear that introducing an iodo-group leads to poorer performances than a bromo-group. On the other hand, LECs containing [Cu(**1**)(POP)]$^+$, [Cu(**1**)(xantphos)]$^+$, [Cu(**2**)(POP)]$^+$, [Cu(**2**)(xantphos)]$^+$, [Cu(**5**)(POP)]$^+$ and [Cu(**5**)(xantphos)]$^+$ exhibited a typical LEC behaviour under bias. This consists of an increase of luminance accompanied by a fast decrease of the voltage. The luminance and voltage behaviours are graphically depicted in Fig. 12 and S14,† respectively, and the performance parameters are summarized in Table 3.

The t_{max} was reached in 6.5, 4.1, 3.2, 1.5, 0.1 and 5.3 h for LECs containing [Cu(**1**)(POP)]$^+$, [Cu(**1**)(xantphos)]$^+$, [Cu(**2**)(POP)]$^+$, [Cu(**2**)(xantphos)]$^+$, [Cu(**5**)(POP)]$^+$ and [Cu(**5**)(xantphos)]$^+$, respectively. Except for complex [Cu(**2**)(POP)]$^+$, the average voltage *versus* time (Fig. S14†) showed a similar behaviour for all devices with an initial fast decay stabilizing in the range 3.9–4.5 V. LECs containing [Cu(**1**)(POP)]$^+$ and [Cu(**1**)(xantphos)]$^+$ (**1** = fluoro-substituted N^N) showed higher Lum_{max} (52 and 129 cd m^{-2}, respectively) when compared to LECs containing [Cu(**2**)(POP)]$^+$ (10 cd m^{-2}), [Cu(**2**)(xantphos)]$^+$ (87 cd m^{-2}), [Cu(**5**)(POP)]$^+$ (14 cd m^{-2}) and [Cu(**5**)(xantphos)]$^+$ (24 cd m^{-2}). Due to the constant current operation, the efficacy values (cd A^{-1}) are directly obtained from the luminance values described above. Hence, LEC containing [Cu(**1**)(xantphos)]$^+$ (fluoro-substituent) showed the maximum efficacy (2.7 cd A^{-1}), power conversion efficiency (PCE = 1.1 lm W^{-1}) and external quantum efficiency (EQE = 0.94%), while the remaining LECs achieved lower efficiencies (Table 3). These results, therefore, indicate that the best LECs are obtained from complexes with the xantphos ligand instead of

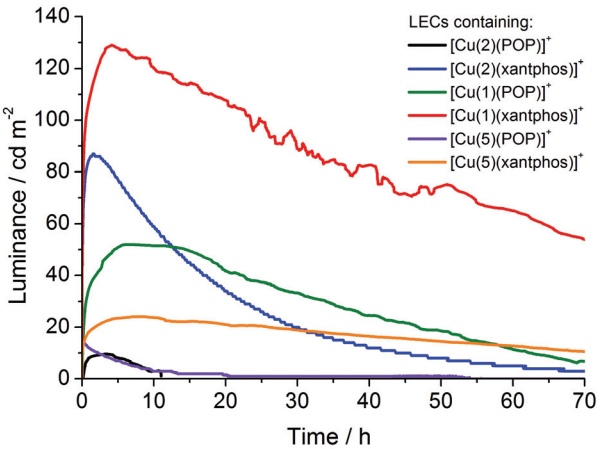

Fig. 12 Luminance for glass/ITO/PEDOT:PSS/active layer/Al devices measured by applying a block-wave pulsed current of 50 A m^{-2} at a frequency of 1 kHz and a duty cycle of 50%. The active layer consisted of different [Cu(N^N)(P^P)][PF_6] complexes mixed with the ionic liquid 1-ethyl-3-methylimidazolium hexafluoridophosphate.

Table 3 Performance parameters obtained for glass/ITO/PEDOT:PSS/active layer/Al devices by applying a block-wave pulsed current of 50 A m^{-2} at a frequency of 1 kHz and duty cycles of 50%. All copper complexes in the emissive layers are $[PF_6]^-$ salts

Complex cation	t_{max} [a]/h	Lum_{max} [b]/cd m^{-2}	$t_{1/2}$ [c]/h	$Efficacy_{max}$ [d]/cd A^{-1}	PCE_{max} [e]/lm W^{-1}	EQE_{max} [f]/%
[Cu(**1**)(POP)]$^+$	6.5	52	38	1.1	0.4	0.38
[Cu(**1**)(xantphos)]$^+$	4.1	129	54	2.7	1.1	0.94
[Cu(**2**)(POP)]$^+$	3.2	10	8.2	0.2	0.1	0.07
[Cu(**2**)(xantphos)]$^+$	1.5	87	15.2	1.8	0.6	0.64
[Cu(**5**)(POP)]$^+$	0.1	14	4.4	0.3	0.1	0.12
[Cu(**5**)(xantphos)]$^+$	5.3	24	61.2	0.5	0.2	0.21

[a] Time to reach Lum_{max}. [b] Maximum luminance. [c] Time to reach one-half of the maximum luminance. [d] Maximum efficacy. [e] Maximum power conversion efficiency. [f] Maximum external quantum efficiency (EQE).

the devices that employ complexes with POP ligands. This is in agreement with the results presented in previous reports.[22,24]

From a comparison of the devices, a trend relating to peripheral halo-substituents can be determined. LECs containing complexes with a fluoro-substituted N^N ligand (LECs with [Cu(**1**)(POP)]$^+$ and [Cu(**1**)(xantphos)]$^+$) performed better than those with analogous chloro-functionalized ligands, which is consistent with the tendency for devices containing the iodo-ligand **4** or the bromo-ligand **3** to perform poorly. Hence, the results show that the LEC performance is strongly influenced by the attached halogen atoms, and improves on going from iodo- to fluoro-functionalization which is in line with the trend for PLQY in thin-films (see Table 2) for each series (**1** > **2** > **3** > **4**). Hence, the observed trend suggests that PLQY is the limiting factor for the electroluminescence behavior of the devices when the ligands are functionalized with I or Br. However, we note that although [Cu(**4**)(xantphos)]$^+$ exhibits a PLQY of 6% in thin films, the LEC containing [Cu(**4**)(xantphos)]$^+$ did not show any electroluminescence whereas this is not the case for [Cu(**2**)(POP)]$^+$ with a PLQY of 4% (thin film). Moreover, [Cu(**3**)(xantphos)]$^+$ with a PLQY of 10% shows a rather poor performance in LECs. The origin of this behaviour remains unclear, but our results are consistent with the detrimental effect observed in LECs employing [Ir(C^N)$_2$(N^N)]$^+$ emitters with a bromophenyl unit in the 4-position of the bpy ligand, which has been reported before.[59] This effect has not been studied in depth.

Conclusions

We report a series of [Cu(N^N)(POP)][PF_6] and [Cu(N^N)(xantphos)][PF_6] complexes in which N^N is either the benchmark ligand **5** (Scheme 1) or is functionalized on the periphery with a halo-substituent (ligands **1–4**). The complexes have been fully characterized by mass spectrometry, solution NMR spectroscopy, and cyclic voltammetry. The single crystal structures of several of the complexes confirm the expected distorted tetrahedral environment of the Cu(I) centre, and the chelating nature of the N^N and P^P ligands. The solution absorption spectra are characterized by high energy bands arising from ligand-centred transitions; these bands are red-shifted on going from [Cu(**5**)(P^P)][PF_6] to [Cu(**1**)(P^P)][PF_6] (**1** contains the fluoro-substituent). A characteristic MLCT band appears around 390 nm for each heteroleptic complex. [Cu(N^N)(POP)][PF_6] and [Cu(N^N)(xantphos)][PF_6] complexes are yellow emitters in solution whilst their powdered samples emit in the yellow or yellow-orange region. Changing the P^P ligand while retaining the same N^N domain has little effect on the solution PL spectrum. Going from [Cu(**5**)(P^P)][PF_6] to [Cu(**1**)(P^P)][PF_6] leads to a red-shift in λ_{em}^{max}. In the solid state, [Cu(**1**)(POP)][PF_6] and [Cu(**1**)(xantphos)][PF_6] (fluoro-substituent) exhibit the highest PL quantum yields (74 and 25%, respectively) with values of $\tau_{1/2}$ = 11.1 and 5.8 μs, respectively. The ten complexes have been tested in the LEC configuration. LECs with the iodo-functionalized ligand **4** did not show any electroluminescence after being under bias for 50 h. An overview of the performance data demonstrates that the introduction of the fluoro-groups is beneficial, and the best performing device employed [Cu(**1**)(xantphos)]$^+$ (Lum_{max} = 129 cd m^{-2} and device $t_{1/2}$ = 54 h); however, a long turn-on time of 4.1 h was observed. We propose that the poor performance of LECs with chloro- or bromo-substituents[59] relates to their lower PL quantum yield in thin films on going from fluoro- to iodo-functionalized ligands.

Acknowledgements

We thank the Swiss National Science Foundation (Grant number 200020_144500), the European Research Council (Advanced Grant 267816 LiLo) and the University of Basel for financial support. We acknowledge financial support from the Spanish Ministry of Economy and Competitiveness (MINECO) *via* the Unidad de Excelencia María de Maeztu MDM-2015-0538, MAT2014-55200. We thank Murat Alkan (University of Basel) for assistance with the program MATLAB.

Notes and references

1 R. D. Costa, E. Ortí, H. J. Bolink, F. Monti, G. Accorsi and N. Armaroli, *Angew. Chem., Int. Ed.*, 2012, **51**, 8178.

2 D. Volz, M. Wallesch, C. Fléchon, M. Danz, A. Verma, J. M. Navarro, D. M. Zink, S. Bräse and T. Baumann, *Green Chem.*, 2015, **17**, 1988.
3 Q. Pei, G. Yu, C. Zhang, Y. Yang and A. J. Heeger, *Science*, 1995, **269**, 1086.
4 H.-C. Su and J.-H. Hsu, *Dalton Trans.*, 2015, **44**, 8330.
5 Y. Zhang and J. Gao, *J. Appl. Phys.*, 2006, **100**, 084501.
6 N. Kaihovirta, C. Larsen and L. Edman, *ACS Appl. Mater. Interfaces*, 2014, **6**, 2940.
7 S. Tang, W.-Y. Tan, X.-H. Zhu and L. Edman, *Chem. Commun.*, 2013, **49**, 4926.
8 M. D. Weber, M. Adam, R. R. Tykwinski and R. D. Costa, *Adv. Funct. Mater.*, 2015, **25**, 5066.
9 M. Y. Wong, G. J. Hedley, G. Xie, L. S. Kolln, I. D. W. Samuel, A. Pertegás, H. J. Bolink and E. Zysman-Colman, *Chem. Mater.*, 2015, **27**, 6535.
10 M. S. Subeesh, K. Shanmugasundaram, C. D. Sunesh, Y. S. Won and Y. Choe, *J. Mater. Chem. C*, 2015, **3**, 4683; K. Shanmugasundaram, M. S. Subeesh, C. D. Sunesh, R. K. Chitumalla, J. Jang and Y. Choe, *Org. Electron.*, 2015, **24**, 297; M. S. Subeesh, K. Shanmugasundaram, C. D. Sunesh, R. K. Chitumalla, J. Jang and Y. Choe, *J. Phys. Chem. C*, 2016, **120**, 12207; K. Shanmugasundaram, M. S. Subeesh, C. D. Sunesh and Y. Choe, *RSC Adv.*, 2016, **6**, 28912.
11 M. D. Weber, V. Nikolaou, J. E. Wittmann, A. Nikolaou, P. A. Angaridis, G. Charalambidis, C. Stangel, A. Kahnt, A. G. Coutsolelos and R. D. Costa, *Chem. Commun.*, 2016, **52**, 1602; K. T. Weber, K. Karikis, M. D. Weber, P. B. Coto, A. Charisiadis, D. Charitaki, G. Charalambidis, P. Angaridis, A. G. Coutsolelos and R. D. Costa, *Dalton Trans.*, 2016, **45**, 13284.
12 J. D. Slinker, A. A. Gorodetsky, M. S. Lowry, J. Wang, S. Parker, R. Rohl, S. Bernhard and G. G. Malliaras, *J. Am. Chem. Soc.*, 2004, **126**, 2763.
13 J.-K. Lee, D. S. Yoo, E. S. Handy and M. F. Rubner, *Appl. Phys. Lett.*, 1996, **69**, 1686.
14 F. G. Gao and A. J. Bard, *J. Am. Chem. Soc.*, 2000, **122**, 7426.
15 S. B. Meier, D. Toreda, A. Pertegás, C. Roldán-Carmona, E. Ortí and H. J. Bolink, *Mater. Today*, 2014, **17**, 217.
16 A. Sandström and L. Edman, *Energy Technol.*, 2015, **3**, 329.
17 B. N. Bideh, C. Roldán-Carmona, H. Shahroosvand and M. K. Nazeeruddin, *Dalton Trans.*, 2016, **45**, 7195 and references therein.
18 J. Slinker, D. Bernards, P. L. Houston, H. D. Abruna, S. Bernhard and G. G. Malliaras, *Chem. Commun.*, 2003, 2392.
19 H. J. Bolink, L. Cappelli, E. Coronado and P. Gaviña, *Inorg. Chem.*, 2005, **44**, 5966.
20 G. Kalyuzhny, M. Buda, J. McNeill, P. Barbara and A. J. Bard, *J. Am. Chem. Soc.*, 2003, **125**, 6272.
21 C. E. Housecroft and E. C. Constable, *Chem. Soc. Rev.*, 2015, **44**, 8386.
22 S. Keller, A. Pertegás, G. Longo, L. Martinez, J. Cerdá, J. M. Junquera-Hernández, A. Prescimone, E. C. Constable, C. E. Housecroft, E. Ortí and H. J. Bolink, *J. Mater. Chem. C*, 2016, **4**, 3857.
23 R. D. Costa, D. Tordera, E. Ortí, H. J. Bolink, J. Schönle, S. Graber, C. E. Housecroft, E. C. Constable and J. A. Zampese, *J. Mater. Chem.*, 2011, **21**, 16108.
24 S. Keller, E. C. Constable, C. E. Housecroft, M. Neuburger, A. Prescimone, G. Longo, A. Pertegás, M. Sessolo and H. J. Bolink, *Dalton Trans.*, 2014, **43**, 16593.
25 N. Armaroli, G. Accorsi, M. Holler, O. Moudam, J. F. Nierengarten, Z. Zhou, R. T. Wegh and R. Welter, *Adv. Mater.*, 2006, **18**, 1313.
26 R. Czerwieniec and H. Yersin, *Inorg. Chem.*, 2015, **54**, 4322.
27 K. Zhang and D. Zhang, *Spectrochim. Acta, Part A*, 2014, **124**, 341.
28 L. Bergmann, J. Friedrichs, M. Mydlak, T. Baumann, M. Nieger and S. Bräse, *Chem. Commun.*, 2013, **49**, 6501.
29 E. Mejía, S.-P. Luo, M. Karnahl, A. Friedrich, S. Tschierlei, A.-E. Surkus, H. Junge, S. Gladiali, S. Lochbrunner and M. Beller, *Chem. – Eur. J.*, 2013, **19**, 15972.
30 X.-L. Chen, R. Yu, Q.-K. Zhang, L.-J. Zhou, X.-Y. Wu, Q. Zhang and C.-Z. Lu, *Chem. Mater.*, 2013, **25**, 3910.
31 A. Kaeser, M. Mohankumar, J. Mohanraj, F. Monti, M. Holler, J.-J. Cid, O. Moudam, I. Nierengarten, L. Karmazin-Brelot, C. Duhayon, B. Delavaux-Nicot, N. Armaroli and J.-F. Nierengarten, *Inorg. Chem.*, 2013, **52**, 12140.
32 C. Femoni, S. Muzzioli, A. Palazzi, S. Stagni, S. Zacchini, F. Monti, G. Accorsi, M. Bolognesi, N. Armaroli, M. Massi, G. Valenti and M. Marcaccio, *Dalton Trans.*, 2013, **42**, 997.
33 I. Andrés-Tomé, J. Fyson, F. Baiao Dias, A. P. Monkman, G. Iacobellis and P. Coppo, *Dalton Trans.*, 2012, **41**, 8669.
34 C. L. Linfoot, M. J. Leitl, P. Richardson, A. F. Rausch, O. Chepelin, F. J. White, H. Yersin and N. Robertson, *Inorg. Chem.*, 2014, **53**, 10854.
35 S.-M. Kuang, D. G. Cuttell, D. R. McMillin, P. E. Fanwick and R. A. Walton, *Inorg. Chem.*, 2002, **41**, 3313.
36 M. D. Weber, C. Garino, G. Volpi, E. Casamassa, M. Milanesio, C. Barolo and R. D. Costa, *Dalton Trans.*, 2016, **45**, 8984.
37 E. Cariatia, E. Lucentib, C. Botta, U. Giovanella, D. Marinotto and S. Righetto, *Coord. Chem. Rev.*, 2015, **306**, 566.
38 D. M. Zink, M. Bächle, T. Baumann, M. Nieger, M. Kühn, C. Wang, W. Klopper, U. Monkowius, T. Hofbeck, H. Yersin and S. Bräse, *Inorg. Chem.*, 2013, **52**, 2292.
39 M. J. Leitl, F.-R. Küchle, H. A. Mayer, L. Wesemann and H. Yersin, *J. Phys. Chem. A*, 2013, **117**, 11823.
40 X.-L. Chen, C.-S. Lin, X.-Y. Wu, R. Yu, T. Teng, Q.-K. Zhang, Q. Zhang, W.-B. Yang and C.-Z. Lu, *J. Mater. Chem. C*, 2015, **3**, 1187.
41 M. J. Leitl, V. A. Krylova, P. I. Djurovich, M. E. Thompson and H. Yersin, *J. Am. Chem. Soc.*, 2014, **136**, 16032.
42 C. L. Linfoot, M. J. Leitl, P. Richardson, A. F. Rausch, O. Chepelin, F. J. White, H. Yersin and N. Robertson, *Inorg. Chem.*, 2014, **53**, 10854.

43 D. G. Cuttell, S.-M. Kuang, P. E. Fanwick, D. R. McMillin and R. A. Walton, *J. Am. Chem. Soc.*, 2002, **124**, 6.
44 H. Yersin, A. F. Rausch, R. Czerwieniec, T. Hofbeck and T. Fischer, *Coord. Chem. Rev.*, 2011, **255**, 2622.
45 F. J. Malzner, S. Y. Brauchli, E. C. Constable, C. E. Housecroft and M. Neuburger, *RSC Adv.*, 2014, **4**, 48712.
46 V.-M. Mukkala and J. J. Kankare, *Helv. Chim. Acta*, 1992, **75**, 1578.
47 B. Bozic-Weber, S. Y. Brauchli, E. C. Constable, S. O. Fürer, C. E. Housecroft and I. A. Wright, *Phys. Chem. Chem. Phys.*, 2013, **15**, 4500.
48 G. J. Kubas, *Inorg. Synth.*, 1979, **19**, 90.
49 *APEX2, version 2 User Manual*, Bruker Analytical X-ray Systems, Inc., M86-E01078, Madison, WI, 2006.
50 P. W. Betteridge, J. R. Carruthers, R. I. Cooper, K. Prout and D. J. Watkin, *J. Appl. Crystallogr.*, 2003, **36**, 1487.
51 I. J. Bruno, J. C. Cole, P. R. Edgington, M. K. Kessler, C. F. Macrae, P. McCabe, J. Pearson and R. Taylor, *Acta Crystallogr., Sect. B: Struct. Sci.*, 2002, **58**, 389.
52 C. F. Macrae, I. J. Bruno, J. A. Chisholm, P. R. Edgington, P. McCabe, E. Pidcock, L. Rodriguez-Monge, R. Taylor, J. van de Streek and P. A. Wood, *J. Appl. Crystallogr.*, 2008, **41**, 466.
53 See for example: N. Armaroli, G. Accorsi, G. Bergamini, P. Ceroni, M. Holler, O. Moudam, C. Duhayon, B. Delavaux-Nicot and J.-F. Nierengarten, *Inorg. Chim. Acta*, 2007, **360**, 1032; K. Saito, T. Arai, N. Takahashi, T. Tsukuda and T. Tsubomura, *Dalton Trans.*, 2006, 4444.
54 J. Yuasa, M. Dan and T. Kawai, *Dalton Trans.*, 2013, **42**, 16096.
55 S. Keller, F. Brunner, A. Prescimone, E. C. Constable and C. E. Housecroft, *Inorg. Chem. Commun.*, 2015, **58**, 64 and references cited therein.
56 B. Bozic-Weber, S. Y. Brauchli, E. C. Constable, S. O. Fürer, C. E. Housecroft, F. J. Malzner, I. A. Wright and J. A. Zampese, *Dalton Trans.*, 2013, **42**, 12293.
57 B. Bozic-Weber, V. Chaurin, E. C. Constable, C. E. Housecroft, M. Meuwly, M. Neuburger, J. A. Rudd, E. Schönhofer and L. Siegfried, *Dalton Trans.*, 2012, **41**, 14157.
58 N. S. Murray, S. Keller, E. C. Constable, C. E. Housecroft, M. Neuburger and A. Prescimone, *Dalton Trans.*, 2015, **44**, 7626.
59 A. M. Bünzli, H. J. Bolink, E. C. Constable, C. E. Housecroft, M. Neuburger, A. Pertegás and J. A. Zampese, *Eur. J. Inorg. Chem.*, 2012, 3780.